Water Research 124 (2017) 372–380

Contents lists available at ScienceDirect

Water Research

journal homepage: www.elsevier.com/locate/watres

Photochlorination-induced transformation of graphene oxide: Mechanism and environmental fate

Tingting Du [a], Adeyemi S. Adeleye [b], Arturo A. Keller [b], Zhineng Wu [a], Wei Han [a], Yingying Wang [a], Chengdong Zhang [a], Yao Li [a, *]

[a] College of Environmental Science and Engineering, Ministry of Education Key Laboratory of Pollution Processes and Environmental Criteria, Tianjin Key Laboratory of Environmental Remediation and Pollution Control, Nankai University, Tong Yan Road 38, Tianjin, 300350, China
[b] Bren School of Environmental Science and Management, University of California, Santa Barbara, CA, 93106, United States

ARTICLE INFO

Article history:
Received 7 May 2017
Received in revised form
11 July 2017
Accepted 21 July 2017
Available online 24 July 2017

Keywords:
Graphene oxide
Transformation
Photochlorination
Antibacterial effect

ABSTRACT

With the increasing production and wide utilization of graphene oxide (GO), the nanomaterials are expected to be released into the environment, and end up in surface waters, and/or wastewater treatment plants. This study explored the changes in the physicochemical properties of GO resulting from photochlorination— simulating the reactions that occur during water and wastewater treatment. Photochlorination resulted in significant changes in the surface oxygen-functionalities of the nanomaterials, and fragmenting of the graphenic carbon sheets was observed. We found that photochlorination can enhance the decomposition of GO through the formation of reduced GO. The changes in surface oxygen-functionalities of GO were attributed to the oxidation by chlorine of the nanomaterials' quinone groups, and further oxidation by Cl• and/or ClO• radicals. The surface charge of GO, measured by its zeta potential, increased in magnitude with chlorination but decreased in magnitude with photochlorination, leading to the decrease in the colloidal stability of the photochlorinated nanomaterials. The antibacterial effect of the nanomaterials increased with both chlorination and photochlorination. This study clearly shows how the physicochemical properties, and environmental fate and effect of GO are modified by photochlorination.

1. Introduction

Graphene oxide (GO), a member of the graphene family nanomaterial, is a functionalized form of graphene, containing epoxy, hydroxyl, carbonyl and carboxyl functional groups (Bai et al., 2011; Lu et al., 2011). GO nanosheet is a unique carbonaceous nanomaterial that possesses excellent electrochemical, optical and mechanical properties. Hence, it has a wide range of applications, including energy storage, biomedicine, and pollution treatment, etc. (Chen et al., 2012; Adeleye et al., 2016; Petridis et al., 2016). The annual production of graphene family nanomaterials was estimated to be 120 metric tons in 2015, and expected to reach 1200 metric tons by 2019 (Zurutuza and Marinelli, 2014; Ciriminna et al., 2015). With the continued increase in production and application of graphene family nanomaterials, it is expected that the nanomaterials will be released into the environment, and may end up in landfills, surface waters, and/or wastewater treatment plants. Accordingly, GO's potential adverse effects to the environment and human health, and its environmental transformations and implications need to be well-understood (Schmidt, 2009).

To date, only a few studies have focused on the transformation of GO in conditions similar and/or relevant to the natural environment (Chowdhury et al., 2015; Feng et al., 2015; Hou et al., 2015, 2016). Some of these studies have shown that sunlight is able to induce some physicochemical changes to the nanomaterials when present in aqueous media. For instance, solar irradiation caused GO to degrade and reduce (to reduced graphene oxide or rGO) (Hou et al., 2015, 2016). The production of CO_2, polycyclic aromatic hydrocarbons (PAHs), and reactive oxygen species (ROS) during solar irradiation of GO was also reported. Despite these existing studies, it is still impossible to predict the fate of these unique materials in most actual aquatic systems. As an example, if present in water treatment systems, GO will also be exposed to other chemicals used in water treatment (e.g. chlorination) in addition to sunlight irradiation.

* Corresponding author.
E-mail address: hkliyao@nankai.edu.cn (Y. Li).

http://dx.doi.org/10.1016/j.watres.2017.07.054
0043-1354/

Chlorination is widely used in drinking water and wastewater (tertiary) treatment (Jiang et al., 2017; Li et al., 2017a, 2017b). If GO is not fully removed during earlier stages of (waste)water treatment, it will reach the chlorine disinfection step where it will be exposed to both disinfection and, perhaps, sunlight irradiation (Gottschalk et al., 2009; Wang et al., 2012b). Chlorination can potentially change the morphology and the oxygen-containing functional groups of carbonaceous materials, including GO (Li et al., 2010; Liu and Zhang, 2014; Stratakis et al., 2014; Savva et al., 2014; Zhai et al., 2014; Du et al., 2016; Li et al., 2016). Concurrent or subsequent sunlight irradiation of chlorinated GO may result in further transformation, affecting further the physicochemical properties (and thus, environmental implications) of GO. This potential transformation of GO by photochlorination has not received much attention as most existing studies on the environmental fate of GO focused on its colloidal stability and sunlight-induced transformations (Chowdhury et al., 2013, 2015; Wu et al., 2013; Hou et al., 2015).

The objectives of the study were to (1) investigate the photochemical transformation of GO during traditional disinfection via photochlorination; and (2) evaluate the colloidal stability and toxicity of GO after photochemical transformations.

2. Material and methods

2.1. Materials and stock preparation

GO nanosheets used in this study were purchased from Plannano Technology Co. (Tianjin, China), and used without further modifications. Based on the information provided by the supplier, the nanosheets were synthesized from graphite using a modified Hummers method (Kotov, 2006). To prepare GO stock suspensions, 400 mg of pristine GO nanosheets were added into 500 mL deionized (DI) water and then ultrasonicated for 4 h at 100 W using a Vibra-Cell VCX800 sonicator (Sonics & Material, Newtown, CT). The GO stock suspension was stored in the dark at 4 °C until use.

The stock of free chlorine solution (1000–3000 mg/L) used in the experiments was prepared from 5% sodium hypochlorite (NaClO; Sigma-Aldrich, St. Louise, MO). The chlorine stock was stored in a flask covered with aluminum foil and kept in the dark at 4 °C. The stock solution was periodically standardized by diethyl-*p*-phenylene diamine (DPD) ferrous titration (American Public Health Association, 1998).

2.2. GO chlorination and photochlorination

Two photochlorinated GO samples were prepared, and two chlorinated GO samples were prepared as a comparison. GO concentration was 10 mg/L for all experiments and the chlorine dosage was either 10 mg/L or 100 mg/L as chlorine (Cl_2). The 10 mg/L Cl_2 dosage was used to simulate the typical chlorine concentration used in water or wastewater disinfection processes (Wang et al., 2006), while the 100 mg/L Cl_2 dosage was used to amplify the effects of chlorination on GO to clearly understand the mechanism. Chlorinated GO samples were kept in the dark throughout the experiment, while photochlorinated GO samples were kept under simulated sunlight for 8 h each day. The samples were buffered at pH 7 with 10 mM phosphate, and total reaction time was 5 d (similar to a previous study) (Li et al., 2016) for all samples. Simulated sunlight irradiation was achieved by placing the reaction quartz flask under a PL-XQ 500W adjustable xenon lamp (Lanpu Co., Shanghai, China) as a light source. The power of xenon lamp used in the study was 420 W and light intensity was 168 mW/cm^2. The light spectrum from the xenon lamp was similar to the summer sunlight spectrum collected in Tianjin, China on May 28, 2015 (Fig. S1).

To stop the chlorination reaction, ascorbic acid (at concentrations 1.2 times of the residual Cl_2, measured with a HACH Cl_2 colorimeter) was added after which the GO samples were cleaned via ultrafiltration and then characterized. Ultrafiltration was done with stirred ultrafiltration cells (Millipore Corporation, Billerica, MA) to remove phosphate buffer, free Cl_2 residuals and other dissolved ions. Detailed information on the ultrafiltration procedure is provided in Supplementary Material section S1.0. The GO samples treated with 10 mg/L and 100 mg/L Cl_2 are hereafter referred to as LCGO and HCGO, respectively. The simulated sunlight-exposed GO samples treated with 10 mg/L and 100 mg/L Cl_2 are hereafter referred to as PLCGO and PHCGO, respectively.

2.3. Material characterization

The functional groups of GOs were characterized via X-ray photoelectron spectroscopy (XPS; PHI 5000 VersaProbe, Japan) and Fourier transform infrared spectroscopy (FTIR; Bruker TENSOR 27, Bruker Optics Inc., Germany). Raman spectra (RM2000 Raman spectrometer, UK) of samples were used to evaluate the defects/changes of GO before and after (photo)chlorination. UV–Vis absorbance spectra of the suspensions were obtained with a UV-2401 spectrophotometer (Shimadzu Scientific Instruments, Columbia, MD). Atomic force microscopy (AFM; MMAFM/STM, D3100M, Digital Ltd., USA) and scanning electron microscopy (SEM; FEI Nova Nano 230, Hillsboro, OR) studies were carried out to analyze the morphology of samples. Total organic carbon (TOC) and inorganic carbon (IC) (multi N/C 3100, Analytik Jena AG, Germany) of GO suspensions were also determined before and after (photo) chlorination.

2.4. Zeta potentials and hydrodynamic diameter (D_h) determination

The surface charge of GO nanomaterials before and after (photo) chlorination treatments were estimated by determining their zeta (ζ) potential using a ZetaSizer Nano ZS (Malvern Instruments, UK). Hydrodynamic size distributions of GO samples were determined before and after (photo)chlorination treatments via dynamic light scattering (DLS) using the ZetaSizer. The pH of GO suspensions was measured using a SevenCompact S230-Basic pH Meter (Mettler-Toledo International Inc., Zurich, Switzerland).

2.5. Antibacterial tests

To investigate the toxicity of (photo)chlorinated GO, a Gram-negative bacterial strain, *Pseudomonas aeruginosa*, was exposed to the transformed nanomaterials in isotonic saline solution. A physiological saline solution containing the same concentration of bacteria and pristine GO was used as a control. The details of bacterial strains cultivation procedure were provided in Supplementary Material section S2.0. After cultivation, the bacteria and GOs mixtures were incubated in a constant temperature (37 °C) incubator with gentle shaking. The total incubation time was 1 h, after which a 1 mL aliquot was drawn out for analyses. Additional experiments were carried out after incubation times of 2 and 3 h for comparison. Antimicrobial activity was analyzed via flow cytometry (FCM) using a CyFlow Space (Sysmex Partec GmbH, Germany) equipped with a 50 mW solid-state laser. Detailed information on FCM measurements was provided in Supplementary Material section S3.0.

3. Results and discussion

3.1. Effects of photochlorination on physical changes of GO

Changes in the physical appearance and morphology of GO after photochlorination were examined. Fig. 1a–e shows the appearance of GO suspensions before and after (photo)chlorination. The appearance of GO suspension clearly changed upon treatment with different concentrations of chlorine, with or without light. The color of GO faded with increased chlorination, as can be seen in the images of LCGO (Fig. 1b) and HCGO (Fig. 1c). This is mainly due to oxidation of GO functional groups by chlorine, which may destruct some chromophore units (such as C=C and C=O groups on the graphitic carbon) (Szpyrkowicz et al., 2001). However, the color trend changed upon the exposure of GO suspensions to light alongside chlorination. While PLCGO was slightly darker than pristine GO (Fig. 1d), but PHCGO was completely clear (Fig. 1e). According to a previous study, sunlight irradiation may reduce GO to reduced GO (rGO), which has a darker color than GO (Hou et al., 2015). Formation of rGO explains the color of PLCGO but not

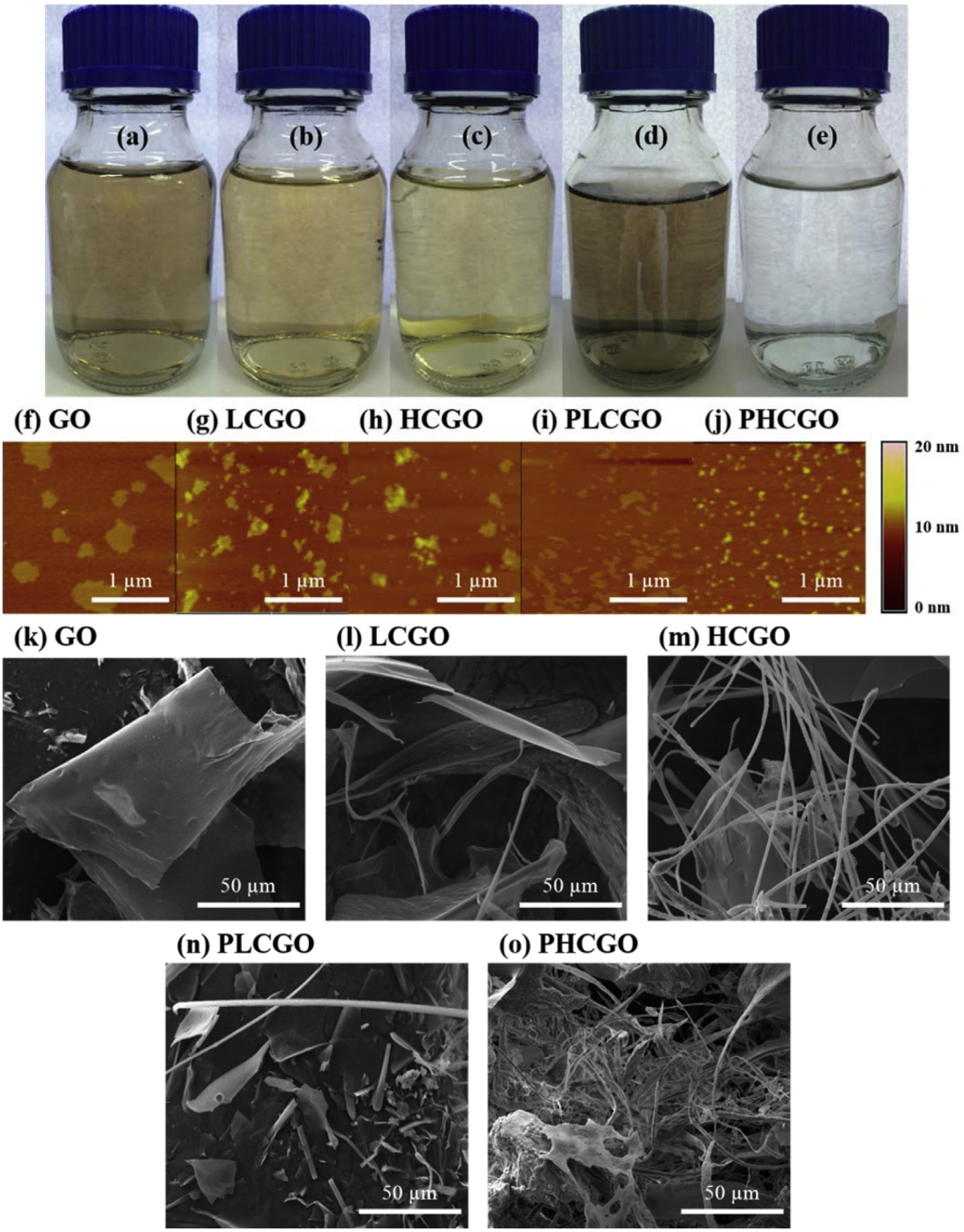

Fig. 1. The photograph of GO suspensions before and after chlorination with and without simulated sunlight exposure: (a) pristine GO, (b) LCGO, (c) HCGO, (d) PLCGO, and (e) PHCGO). AFM micrographs of GOs upon chlorination with or without light irradiation: (f) pristine GO, (g) LCGO, (h) HCGO, (i) PLCGO, and (j) PHCGO. SEM images of GOs upon chlorination with or without light irradiation: (k) pristine GO (l) LCGO, (m) HCGO, (n) PLCGO and (o) PHCGO. (Reaction time = 5 d at 8 h/d).

PHCGO.

The AFM micrographs (Fig. 1f–j) show that GO nanoplatelets were damaged at the edges after mild or heavy (photo)chlorination, and the GO nanoplatelets were heavily fragmented by photochlorination (Fig. 1i–j), especially with high Cl_2 concentration (PHCGO sample). SEM images (Fig. 1k–o) further prove the changes in the morphology of GO after treatment with chlorination and photochlorination. It should be noted that several of the extremely small fragments formed after the treatments may have been removed during the ultrafiltration step in the sample preparation. Scrolled GO sheets in the LCGO and HCGO samples, which were also found in our previous study (Li et al., 2010), may be due to asymmetric distributions of cations, creating a polarization that is relieved by curling (Schaak and Mallouk, 2000). The fragmentation of chlorinated GO nanosheets appeared to be intensified upon irradiation as can be seen in the much smaller sizes of PLCGO and PHCGO samples (Fig. 1n and o), which agrees well with AFM data. However, much more scrolled GO in the PHCGO sample also emphasize the importance of chlorination procedure in the photochlorination procedure.

3.2. Effects of photochlorination on chemical properties of GO

The influence of photochlorination on the surface chemistry of GO was evaluated via XPS, FTIR, Raman, and UV–Vis spectrometric analyses. Comparisons of the XPS survey and high resolution spectra of GO, LCGO, HCGO, PLCGO, and PHCGO are shown in Fig. 2a–f. In the high resolution spectra, the C1s peaks located at binding energy (BE) of 284.5 eV, 286.7 eV, 287.8 eV, and 288.8 eV were assigned to the carbon atoms or oxygen-functional group in aromatic rings (C–C/C=C), hydroxyl or epoxy (C–OH/C–O–C), carbonyl (C=O), and carboxyl (O–C=O), respectively (Fig. 2a–e) (Chandra et al., 2010).

Quantitative analyses of these carbon species (Fig. 2g) showed that (in comparison to pristine GO) the fraction of C–OH/C–O–C and O–C=O groups increased in the LCGO samples, whereas the fraction of C=O group decreased. However, in HCGO samples, only the fraction of O–C=O groups increased, while C–OH/C–O–C and C=O groups decreased. The O/C ratio of LCGO and HCGO samples was similar to that of pristine GO, indicating that little or no further addition of new oxygen groups to the graphitic layers occurred upon 10 and 100 mg/L chlorine treatments. The decrease of C–OH groups and increase of O–C=O groups in HCGO sample suggests further oxidation of C–OH functional group to O–C=O functional group in the presence of higher concentrations of chlorine.

In contrast, the ratio of C–C/C=C groups in PLCGO and PHCGO increased significantly (Fig. 2g), which suggests decomposition (loss) of some of the oxygen-containing functional groups in GO (e.g., C–OH/C–O–C) due to sunlight irradiation. As shown in the XPS survey spectra of the different GOs in Fig. 2f, a peak for C–Cl (or Cl–C=O) bond with BE of ~200.3 eV emerged after (photo)chlorination (Kim et al., 2013; Zhang et al., 2013). The strongest C–Cl/Cl–C=O peak was found in the PHCGO sample, which indicates that simulated sunlight irradiation enhanced the chlorination of GO at

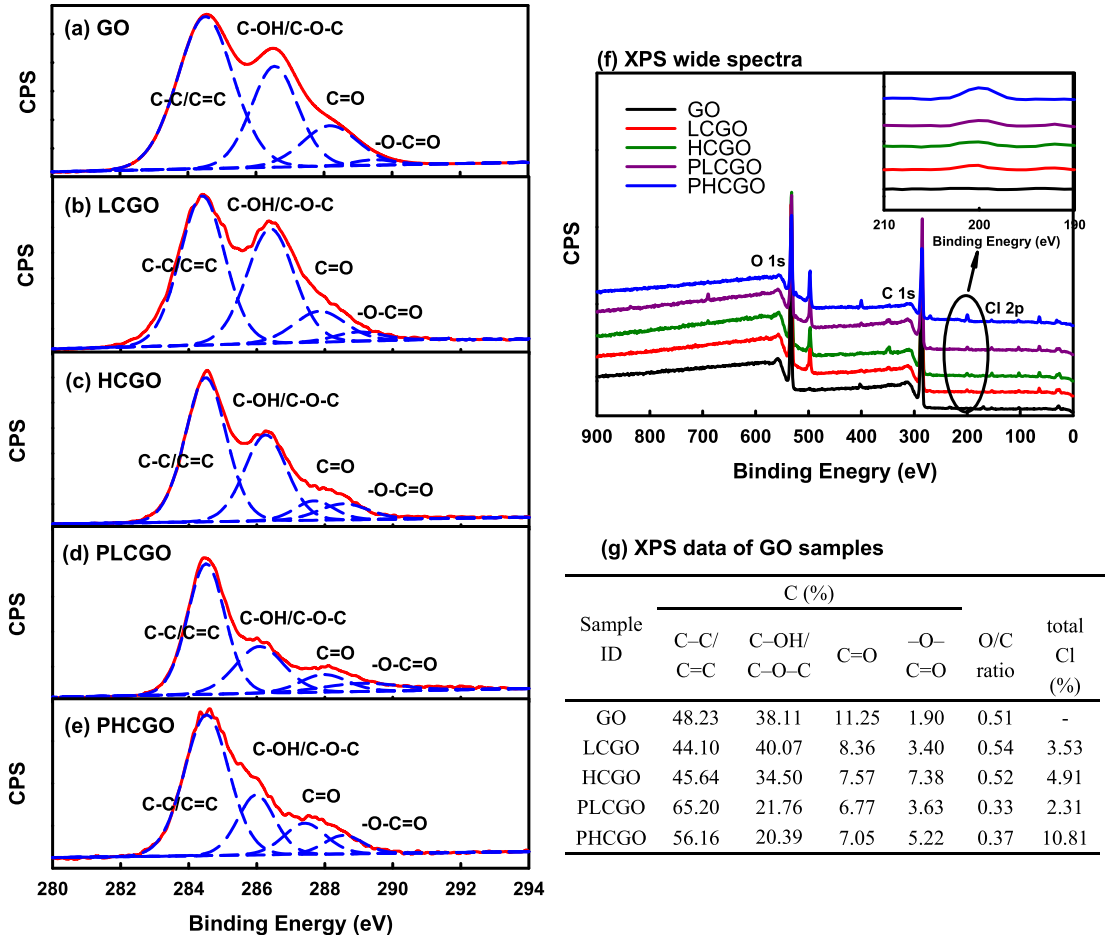

(g) XPS data of GO samples

Sample ID	C (%)				O/C ratio	total Cl (%)
	C–C/C=C	C–OH/C–O–C	C=O	–O–C=O		
GO	48.23	38.11	11.25	1.90	0.51	-
LCGO	44.10	40.07	8.36	3.40	0.54	3.53
HCGO	45.64	34.50	7.57	7.38	0.52	4.91
PLCGO	65.20	21.76	6.77	3.63	0.33	2.31
PHCGO	56.16	20.39	7.05	5.22	0.37	10.81

Fig. 2. X-ray photoelectron spectroscopy (XPS) analysis of GO before and after chlorine treatment with or without light irradiation. High resolution XPS spectra of the C 1s peaks of pristine GO (a), LCGO (b), HCGO (c), PLCGO (d) and PHCGO (e). (f) XPS survey spectra of all the GO nanosheets. (g) Quantitation of C1s peaks of the GO samples.

the high chlorine concentration treatment.

Changes in the surface chemistry of GO upon photochlorination were further characterized by FTIR (Fig. 3a and b). Pristine GO exhibited four characteristic peaks located at 612, 1383, 1628 and 1735 cm^{-1}, corresponding to C–C vibration (Kratschmer et al., 1990), hydroxyl group (O–H bending band), carboxyl group stretching, and C=O stretching, respectively (Hontoria-Lucas et al., 1995; Acik et al., 2011; Li et al., 2012). After GO reacted with free Cl_2 (10 mg/L or 100 mg/L) for 5 d, the peak for C=O stretching in GO decreased, while the peaks for C–OH and O–C=O functional groups increased, indicating a transformation of C=O groups to O–C=O and C–OH groups. In addition, two new peaks were observed (at 798 and 1100 cm^{-1}, which are typical of C–Cl stretching and aryl C–Cl, respectively (Salavagione and Martinez, 2011; Wang et al., 2012a). This suggests that one of the most important outcomes of the reaction of GO with Cl_2 is the incorporation of Cl atoms into unsaturated ethylic sites of GO aromatic rings. Changes in the surface chemistry of GO after photochlorination, observed via FTIR, were very similar to the changes observed with only chlorination. The most obvious difference observed between chlorination and photochlorination was a significantly larger peak at 1100 cm^{-1} (assigned to aryl C–Cl group) on the PHCGO sample, which may due to enhanced chlorination of GO in the presence of irradiation as also observed with XPS analysis.

Raman spectra of pristine, chlorinated and photochlorinated GOs are shown in Fig. 3c. The ratio of the D band (1360 cm^{-1}), which measures the presence of disorder in sp^2-hybridized carbon systems, to G band (1590 cm^{-1}) that evaluates stretching of C–C bonds in graphitic materials, (I_D/I_G), were compared (Dresselhaus et al., 2010). The I_D/I_G value of all treated GO increased compared to that of pristine GO. The highest increases in I_D/I_G values were observed in PLCGO (increased by 0.15) and PHCGO (increased by 0.16) samples, which indicates that many more defects were formed on GO after photochlorination (compared to chlorination alone where the increase in I_D/I_G was <0.1).

The UV–Vis spectra of all the samples are shown in Fig. 3d. The characteristic absorbance peak of GO at 230 nm was detected in pristine GO, LCGO and HCGO samples. However, the peak (and thus, GO concentration) decreased sharply in samples treated with chlorine and simulated sunlight (i.e., PLCGO and PHCGO), which is quite different from the results observed when GO was only subjected to irradiation in a previous study (Hou et al., 2015). This result suggests that some decomposition of GO occurred in the presence of both chlorine and sunlight, but not (or much less so) in chlorine alone. In addition, a peak around 300 nm (which represents residual chlorine) was observed in the HCGO sample, mainly due to high Cl_2 concentration used in that condition (Watts and Linden, 2007). However, a similar residual chlorine peak was not observed in PHCGO (which was also treated with a similar level of Cl_2 as HCGO), suggesting a transformation of residual chlorine under sunlight irradiation.

3.3. Mechanisms controlling GO transformation by photochlorination

Based on the spectroscopic and electron microscopic analyses, we believed that chlorination and/or sunlight irradiation are effective in changing the surface chemistry and morphology of GO.

HClO, a weak acid produced from chlorine in water, cannot substantially further increase the oxygen content of GO upon chlorination treatments although we observed the oxidation of quinone/carbonyl groups on the basal plane or edges of GO to epoxy, hydroxyl, and carboxyl groups (as shown by XPS and FTIR). Rather, chlorination of GO led to electrophilic additions of chlorine

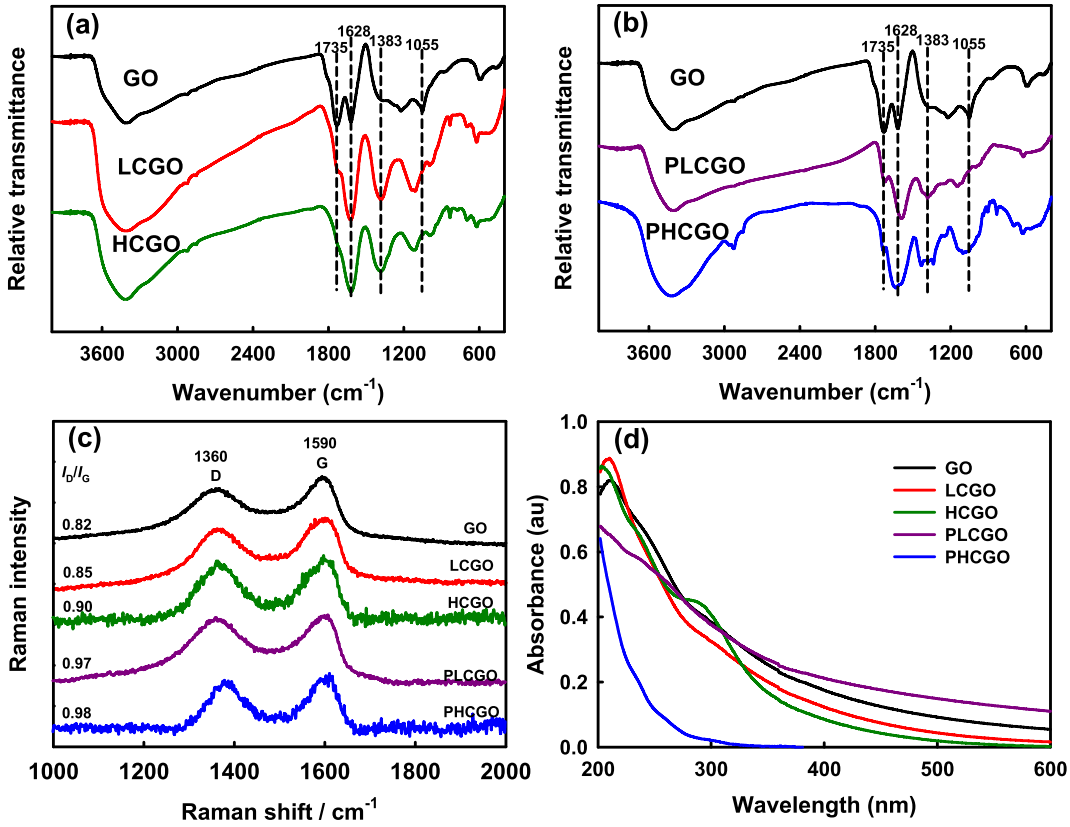

Fig. 3. (a–b) Fourier transform infrared (FT-IR) spectra, (c) Raman spectra, (d) UV–Vis spectra of GO, LCGO, HCGO, PLCGO and PHCGO.

atoms at the unsaturated sites of GO's benzene ring (Li et al., 2016). Higher HClO dosage had additional effects on GO's surface chemistry, such as further oxidation of hydroxyl groups to carboxyl groups (Sivey and Roberts, 2012). However, neither HClO nor aqueous Cl_2 was reactive enough to break GO's carbon platelets and add new oxygen functional groups onto them.

According to Hou and co-workers, irradiation led to the disproportionation of GO to CO_2, photoproducts similar to reduced GO, and PAH-like materials (Hou et al., 2015). Similarly, we observed the production of CO_2 (inorganic carbon) and reduction of GO to rGO upon photochlorination of GO in this study (Fig. S2). CO_2 was formed from the oxidation of the unsaturated oxygen-containing functional groups on GO. The formation and release of CO_2 from GO platelets led to the fragmentation of the platelets, and the reduction of the oxygen-containing functional groups. However, the characterization results indicate that the effects of photochlorination on GO were much complicated, including other important reactions.

As a photo-reactive semiconductor, irradiation of GO results in the formation of oxidative (valence band holes, h^+_{vb}) and reductive (conduction band electron, e^-_{aq}) transients (Hou et al., 2015). These co-occurring transients react with dissolved oxygen in water to yield reactive oxygen species (ROS) such as $^1O_2$, •OH and $O_2^{\bullet-}$. The h^+_{vb} may easily affect the oxidation of O-functional groups, while e^-_{aq} promotes the formation of of C—Cl. Meanwhile, photolysis of aqueous Cl_2 occurs when irradiated at wavelengths below 511 nm to form chlorine radicals (Cl•) and hydroxyl radicals (•OH) as shown in Equation (1) (Carrión et al., 1972; Nowell and Hoigné, 1992; Cataldo, 1994; Wang et al., 2012a; Zhao et al., 2011):

$$HClO(ClO^-) \xrightarrow{h\nu} {}^{\bullet}OH\ (O^{\bullet-}) + Cl^{\bullet} \quad (1)$$

Cl• and •OH could further react with aqueous Cl_2 to form oxychlorine radicals (ClO•) (Carrión et al., 1972; Nowell and Hoigné, 1992). Unlike HClO, ClO^- and aqueous Cl_2 species that are formed from NaClO in the absence of light, Cl• and ClO• that are formed during irradiation are much more reactive with GO particles during photochlorination. Weak oxidants, HClO, ClO^- (formed during chlorination), contribute to the formation of C—Cl and —COOH bonds at the edges of GO. Cl• and ClO•, which are formed when irradiation is coupled with chlorination, are stronger oxidants, and may easily attack GO at its reactive sites (including e^-_{aq}) and even some nonreactive sites to form C—Cl and Cl—C=O bonds. The deconvolution of Cl 2p XPS peak showed the presence of C—Cl (BE = 200.3 eV) and Cl—C=O (BE = 202 eV) bonds in PLCGO and PHCGO samples; but Cl—C=O bonds were not present in samples treated only with chlorination (Fig. 4). As such, under sunlight irradiation, Cl_2 species/radicals species can attack both the edges and basal plane of GO sheets, while the basal plane is less vulnerable without irradiation.

Based on the results in this study and analysis above, we believe that the chlorination and irradiation effects are both important during the photochlorination procedure, but the dominant factor depends on chlorine concentrations. At low concentrations (such as 10 mg/L), chlorine was completely decomposed by irradiation to form Cl• and ClO• radicals. Although Cl• and ClO• are strong oxidants, their low concentrations limited their effects and the formation of C-Cl/C-Cl=O bonds. As a result, irradiation was the more dominant factor in the transformation of PLCGO samples. At much higher chlorine dosage (100 mg/L), however, much more Cl• and ClO• were formed during the irradiation of chlorine. High concentrations of HClO, Cl_2, Cl• and ClO• resulted in the formation of C-Cl/C-Cl=O bonds on the reactive sites within GO's fragmented sheets. The possible scheme of photochlorination of GO is shown in Fig. 5. In the natural environment, other factors including pH, ions, and natural organic matter (NOM) will also play a role in the photochlorination of GO. In

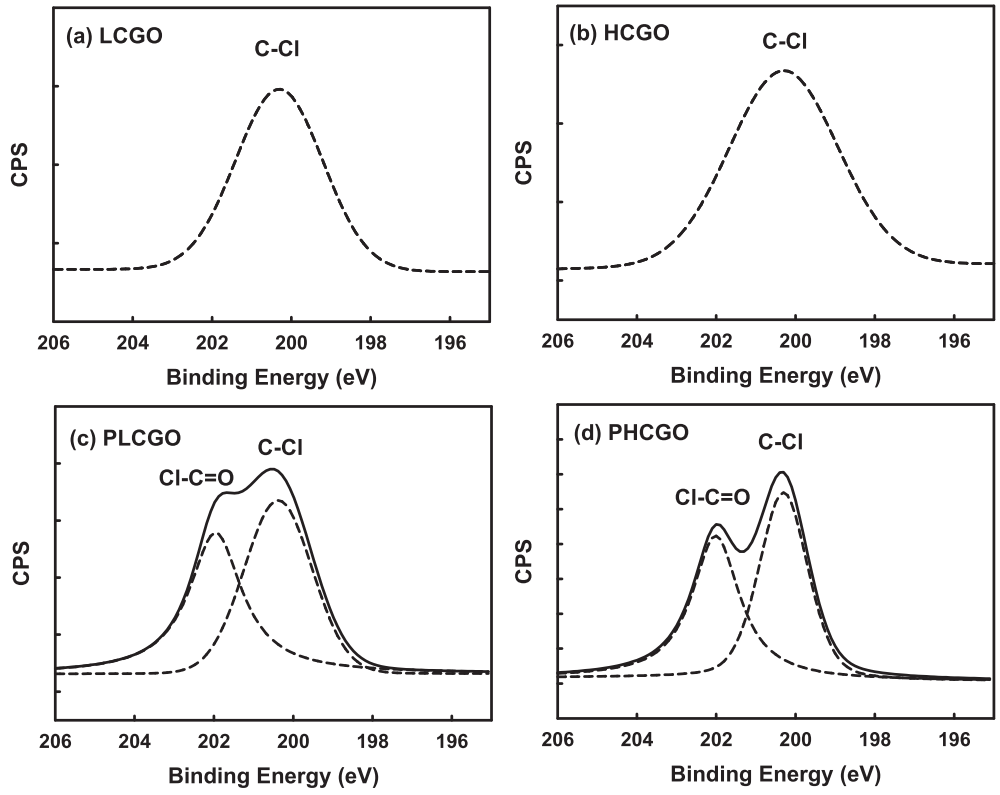

Fig. 4. High-resolution XPS spectra of the Cl 2p peak for (photo)chlorinated GO. Deconvolution revealed the presence of Cl—C (200.3 eV) and Cl—C=O (202 eV) groups.

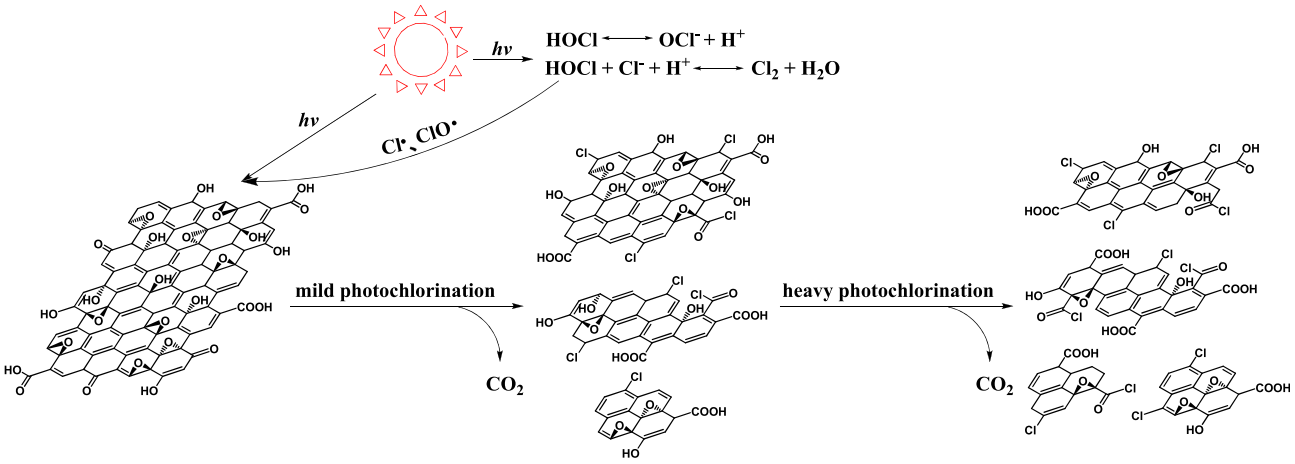

Fig. 5. Proposed mechanism of photochlorination of graphene oxide nanosheet.

particular, NOM may affect the transformation of GO in two possible ways: (1) NOM may coat GO nanosheets (Chowdhury et al., 2015) and thereby attenuate the effects of direct irradiation, and thus, decomposition of GO; and (2) NOM could also consume aqueous chlorine and other chlorine radicals (Li et al., 2017a), minimizing the formation of C-Cl/C-Cl=O bonds on the surface of GO.

3.4. Effect of (photo)chlorination on colloidal stability of GO suspensions

The ζ potential and size distribution of GO before and after the (photo)chlorination were shown in Fig. 6. ζ potential of GO increased in magnitude from −45 to −50 mV after chlorination, and decreased to −40 mV after photochlorination (Fig. 6a). Chlorination led to the oxidation of the −OH group on the surface of GO to −COOH group, which may lead to increase in the pH of GO suspension. Photochlorination of GO may also lead to increase in pH since −OH group was further oxidized. The pH of GO suspensions increased from 5 to a range of 8–10 (after chlorination) or a range of 5–7 (after photochlorination) as shown in Fig. S3. Both increase in −COOH group and elevated pH led to increases in the magnitude of ζ potential observed in the (photo)chlorination treated samples. However, light-induced dispropornation of GO led to decrease in the ζ potential of GO, making the nanosheets potentially less stable in aquatic systems. However, the ζ potential of GO exceeded −30 mV (the typical threshold of colloidal stability (Everett, 1988)) in all the treatments indicating that the GO photo-transformation products were still reasonably stable.

DLS data showed that the hydrodynamic diameter of GO was not substantially changed upon (photo)chlorination. As shown in Fig. 6b, the size distributions of GO suspensions were similar before (GO) and after chlorination (LCGO and HCGO). Bimodal size distribution was observed in PLCGO and PHCGO with the new size distribution peak appearing at sizes smaller than that of pristine GO. This also agrees with microscopic data that showed degradation of GO sheets to smaller sizes after photochlorination.

3.5. The toxic effects of (photo)chlorinated GO

The toxic effects of all the GO samples, measured by death rate, to *P. aeruginosa* was determined and shown in Fig. 7. In order to clearly see the antibacterial effect of GO samples, 100 mg/L GO was used in the experiment. Antimicrobial activity which was analyzed via flow cytometry (FCM) was shown in Fig. 7a. Bacterial death rate, resulting from 1 h of contact time with the nanomaterials, increased significantly from 15% when exposed to pristine GO to ~20% ($p < 0.05$) and ~30% ($p < 0.05$) when the cells were exposed to GO nanosheets treated with low dosage of Cl_2 (LCGO) and high dosage of Cl_2 (HCGO), respectively. Toxicity did not increase any further when the cells were exposed to GO samples that were simultaneously exposed to chlorination and sunlight irradiation (Fig. 7b). In fact, death rates were significantly less ($p < 0.05$) in PHCGO than in HCGO. The highest toxicity was observed in HCGO

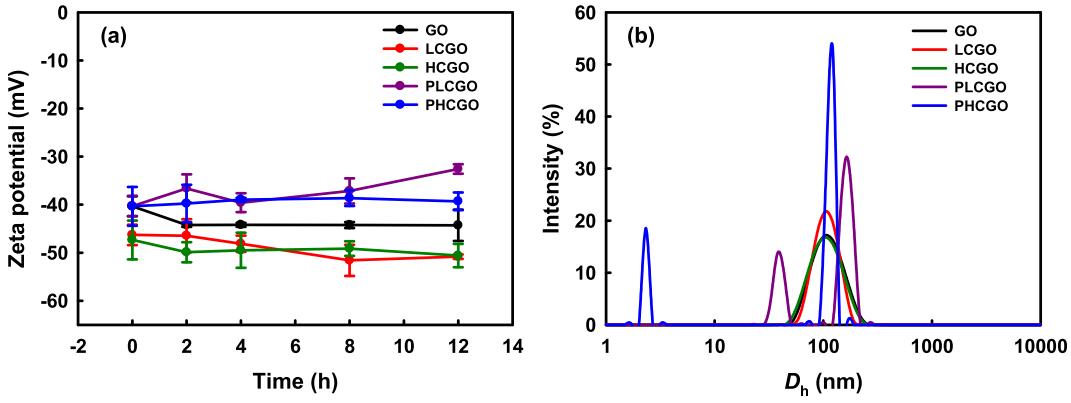

Fig. 6. (a) Zeta potential, and (b) Size distribution of GO before and after (photo)chlorination. GO concentration = 10 mg/L.

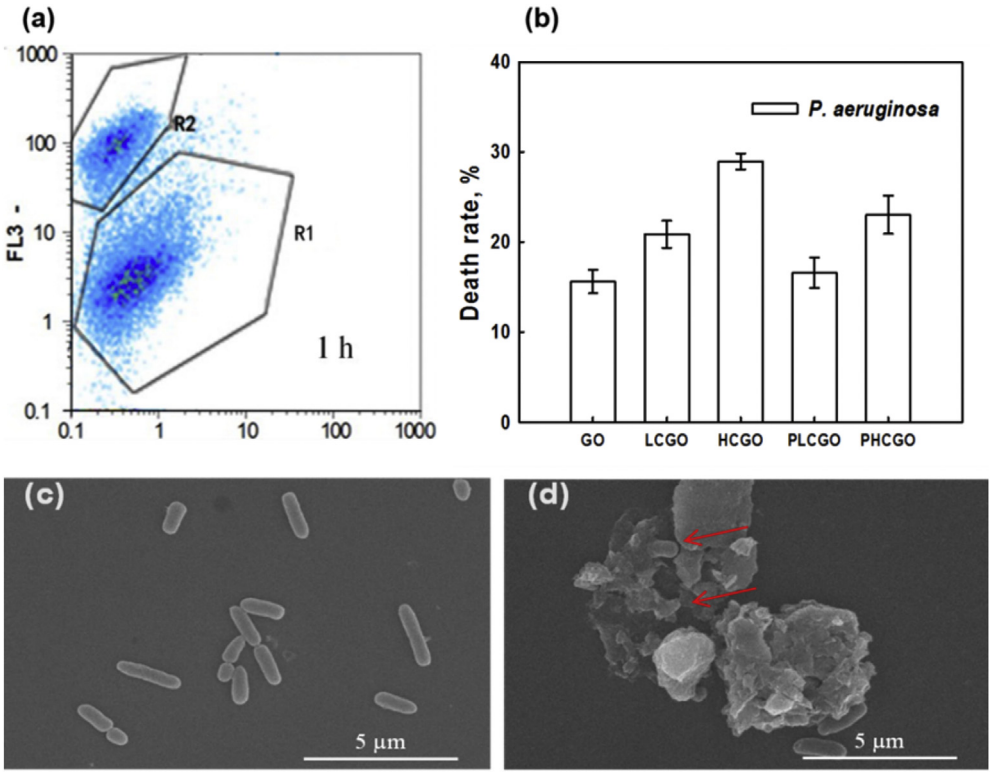

Fig. 7. (a) A typical flow cytometry (FCM) image of antibacterial activity of GO samples to *P. aeruginosa*. R1 represents live bacteria and R2 represents dead bacteria. (Contact time = 1 h), and (b) Effect of (photo)chlorination on the toxicity of GO to *P. aeruginosa* cells. (GO concentration = 100 mg/L; contact time = 1 h; pH = 7). SEM images of *P. aeruginosa* before (c) and after (d) contact with chlorinated GOs (arrows show some sliced bacterial cells).

samples. Further studies showed that the antibacterial effect of GO to the bacterium was both concentration- and exposure time-dependent (Figs. S4 and S5).

Generally, the antimicrobial effects of GO materials have been proposed to occur via three major mechanisms: (1) acting as *nanoknives* due to their sharp edges (Chen et al., 2013, 2014; Wang et al., 2013; He et al., 2015), (2) oxidative stress mediated with or without the production of ROS (Lewinski et al., 2008; Liu et al., 2013; Smith and Rodrigues, 2015), and (3) reduction of nanomaterials, which may decrease their stability, and thus the concentration on the bacteria due to heteroaggregation (Carpio et al., 2012; Perreault et al., 2015). As shown in Fig. 7c–d, SEM images provided evidence for slicing of bacterial cells by GO in this study (*nanoknives* effect). As explained earlier, chlorination of GO resulted in scrolling and increased defect at the edges; while photochlorination mainly led to defects on the edges and basal planes as well as fragmentation. In addition, photochlorinated GO was also reduced compared to the GO exposed to only chlorination. The scrolling of GO nanosheets may decrease their ability to act as a nanoknifes but fragmentation and increased edge defects enhanced the antimicrobial effects of GO (Poland et al., 2008; Yang and Ma, 2010; Perreault et al., 2015). The results indicate that the defects from chlorination procedure may highly increase the antibacterial effects of GO, but the reduction (with photochlorination) may inhibit them. In this study, we only provided a preliminary investigation of the effect of (photo)chlorination-induced transformation on the antimicrobial properties of GO but further studies are needed to fully understand the mechanisms.

4. Conclusions

Release of graphene oxide nanosheets into water and wastewater treatment plants will facilitate some physicochemical transformations of the nanomaterials due to the exposure of the nanomaterials to chlorination and irradiation. This study showed that the oxygen-containing groups of graphene oxide were either transformed during chlorination, or simultaneously transformed and reduced when chlorination was combined with sunlight irradiation (as we would expect to occur in wastewater treatment plants). These chemical changes led to physical changes in the nanosheets—mainly scrolling and fragmentation to much smaller sizes. These changes influenced media pH, and nanomaterial size distribution, surface charge, and antibacterial effects. Although not tested in this study, the changes will also affect other processes such nanomaterial aggregation, adsorption, transport, and interactions with other surfaces (geogenic and biogenic), etc.

Acknowledgments

This project was supported by the Ministry of Science and Technology of China (Grant 2014CB932001, 2015CB459000), and the National Natural Science Foundation of China (Grants 21677078, 81373039 and 31322012).

Appendix A. Supplementary data

Supplementary data related to this article can be found at http://dx.doi.org/10.1016/j.watres.2017.07.054.

References

Acik, M., Lee, G., Mattevi, C., Pirkle, A., Wallace, R.M., Chhowalla, M., Cho, K., Chabal, Y., 2011. The role of oxygen during thermal reduction of graphene oxide studied by infrared absorption spectroscopy. J. Phys. Chem. C 115 (40), 19761–19781.

Adeleye, A.S., Conway, J.R., Garner, K., Huang, Y., Su, Y., Keller, A.A., 2016. Engineered nanomaterials for water treatment and remediation: costs, benefits, and applicability. Chem. Eng. J. 286, 640–662.
American Public Health Association, A.W.W.A., Water Environment Federation, 1998. In: Association, A.P.H. (Ed.), Standard Methods for the Examination of Water and Wastewater, twentieth ed. Washington, DC.
Bai, H., Li, C., Wang, X., Shi, G., 2011. On the gelation of graphene oxide. J. Phys. Chem. C 115 (13), 5545–5551.
Carpio, I.E.M., Santos, C.M., Wei, X., Rodrigues, D.F., 2012. Toxicity of a polymer-graphene oxide composite against bacterial planktonic cells, biofilms, and mammalian cells. Nanoscale 4 (15), 4746–4756.
Carrión, D.M.R., Montalvo, S.S., Martínez-Taboas, A., 1972. Radiation chemistry and photochemistry of oxychlorine ions. Part 1. Radiolysis of aqueous solutions of hypochlorite and chlorite ions. J. Chem. Soc. Faraday Trans. 68 (68), 947–957.
Cataldo, F., 1994. Photochlorination of C_{60} and C_{70} fullerenes. Carbon 32 (3), 437–443.
Chandra, V., Park, J., Chun, Y., Lee, J.W., Hwang, I., Kim, K.S., 2010. Water-dispersible magnetite-reduced graphene oxide composites for arsenic removal. Acs Nano 4 (7), 3979–3986.
Chen, D., Feng, H., Li, J., 2012. Graphene oxide: preparation, functionalization, and electrochemical applications. Chem. Rev. 112 (11), 6027–6053.
Chen, J.N., Peng, H., Wang, X.P., Shao, F., Yuan, Z.D., Han, H.Y., 2014. Graphene oxide exhibits broad-spectrum antimicrobial activity against bacterial phytopathogens and fungal conidia by intertwining and membrane perturbation. Nanoscale 6 (3), 1879–1889.
Chen, J.N., Wang, X.P., Han, H.Y., 2013. A new function of graphene oxide emerges: inactivating phytopathogenic bacterium Xanthomonas oryzae pv. oryzae. J. Nanopart. Res. 15 (5).
Chowdhury, I., Duch, M.C., Mansukhani, N.D., Hersam, M.C., Bouchard, D., 2013. Colloidal properties and stability of graphene oxide nanomaterials in the aquatic environment. Environ. Sci. Technol. 47 (12), 6288–6296.
Chowdhury, I., Hou, W., Goodwin, D., Henderson, M., Zepp, R.G., Bouchard, D., 2015. Sunlight affects aggregation and deposition of graphene oxide in the aquatic environment. Water Res. 78, 37–46.
Ciriminna, R., Zhang, N., Yang, M.Q., Meneguzzo, F., Xu, Y.J., Pagliaro, M., 2015. Commercialization of graphene-based technologies: a critical insight. Chem. Commun. 51 (33), 7090–7095.
Dresselhaus, M.S., Jorio, A., Hofmann, M., Dresselhaus, G., Saito, R., 2010. Perspectives on carbon nanotubes and graphene raman spectroscopy. Nano Lett. 10 (3), 751–758.
Du, T., Wang, Y., Yang, X., Wang, W., Guo, H., Xiong, X., Gao, R., Wuli, X., Adeleye, A.S., Li, Y., 2016. Mechanisms and kinetics study on the trihalomethanes formation with carbon nanoparticle precursors. Chemosphere 154, 391–397.
Everett, D., 1988. Basic Principles of Colloid Science. Royal Society of Chemistry.
Feng, Y., Lu, K., Mao, L., Guo, X., Gao, S., Petersen, E.J., 2015. Degradation of C-14-labeled few layer graphene via Fenton reaction: reaction rates, characterization of reaction products, and potential ecological effects. Water Res. 84, 49–57.
Gottschalk, F., Sonderer, T., Scholz, R.W., Nowack, B., 2009. Modeled environmental concentrations of engineered nanomaterials (TiO_2, ZnO, Ag, CNT, Fullerenes) for different regions. Environ. Sci. Technol. 43 (24), 9216–9222.
He, J.L., Zhu, X.D., Qi, Z.N., Wang, C., Mao, X.J., Zhu, C.L., He, Z.Y., Lo, M.Y., Tang, Z.S., 2015. Killing dental pathogens using antibacterial graphene oxide. Acs Appl. Mater. Inter. 7 (9), 5605–5611.
Hontoria-Lucas, C., López-Peinado, A.J., López-González, J.D.D., Rojas-Cervantes, M.L., Martín-Aranda, R.M., 1995. Study of oxygen-containing groups in a series of graphite oxides: physical and chemical characterization. Carbon 33 (11), 1585–1592.
Hou, W., Chowdhury, I., Goodwin, D., Henderson, M., Fairbrother, D.H., Bouchard, D., Zepp, R.G., 2015. Photochemical transformation of graphene oxide in sunlight. Environ. Sci. Technol. 49 (6), 3435–3443.
Hou, W., Henderson, W.M., Chowdhury, I., Goodwin Jr., D.G., Chang, X., Martin, S., Fairbrother, D.H., Bouchard, D., Zepp, R.G., 2016. The contribution of indirect photolysis to the degradation of graphene oxide in sunlight. Carbon 110, 426–437.
Jiang, J.Y., Zhang, X.R., Zhu, X.H., Li, Y., 2017. Removal of intermediate aromatic halogenated DBPs by activated carbon adsorption: a new approach to controlling halogenated DBPs in chlorinated drinking water. Environ. Sci. Technol. 51 (6), 3435–3444.
Kim, J., Lee, W., Suk, J.W., Potts, J.R., Chou, H., Kholmanov, I.N., Piner, R.D., Lee, J., Akinwande, D., Ruoff, R.S., 2013. Chlorination of reduced graphene oxide enhances the dielectric constant of reduced graphene oxide/polymer composites. Adv. Mater. 25 (16), 2308–2313.
Kotov, N.A., 2006. Materials science: carbon sheet solutions. Nature 442 (7100), 254–255.
Kratschmer, W., Lamb, L.D., Fostiropoulos, K., Huffman, D.R., 1990. Solid C_{60} : a new form of carbon. Nature 347 (6291), 354–358.
Lewinski, N., Colvin, V., Drezek, R., 2008. Cytotoxicity of nanoparticles. Small 4 (1), 26–49.
Li, M., Cushing, S.K., Zhou, X., Guo, S., Wu, N., 2012. Fingerprinting photoluminescence of functional groups in graphene oxide. J. Mater. Chem. 22 (44), 23374–23379.
Li, Y., Yang, M.T., Zhang, X.R., Jiang, J.Y., Liu, J.Q., Yau, C.F., Graham, N.J.D., Li, X.Y., 2017a. Two-step chlorination: a new approach to disinfection of a primary sewage effluent. Water Res. 108, 339–347.
Li, Y., Yang, N., Du, T., Wang, X., Chen, W., 2016. Transformation of graphene oxide by chlorination and chloramination: implications for environmental transport and fate. Water Res. 103, 416–423.
Li, Y., Zhang, X.R., Shang, C., 2010. Effect of reductive property of activated carbon on total organic halogen analysis. Environ. Sci. Technol. 44 (6), 2105–2111.
Li, Y., Zhang, X.R., Yang, M.T., Liu, J.Q., Graham, N.J.D., Li, X.Y., Yang, B., 2017b. Three-step chlorination increases disinfection efficiency and reduces DBP formation and toxicity. Chemosphere 168, 1302–1308.
Liu, J.Q., Zhang, X.R., 2014. Comparative toxicity of new halophenolic DBPs in chlorinated saline wastewater effluents against a marine alga: halophenolic DBPs are generally more toxic than haloaliphatic ones. Water Res. 65, 64–72.
Liu, Y., Zhao, Y.L., Sun, B.Y., Chen, C.Y., 2013. Understanding the toxicity of carbon nanotubes. Acc. Chem. Res. 46 (3), 702–713.
Lu, N., Yin, D., Li, Z., Yang, J., 2011. Structure of graphene oxide: thermodynamics versus kinetics. J. Phys. Chem. C 115 (24), 11991–11995.
Nowell, L.H., Hoigné, J., 1992. Photolysis of aqueous chlorine at sunlight and ultraviolet wavelengths-II. Hydroxyl radical production. Water Res. 26 (5), 599–605.
Perreault, F., de Faria, A.F., Nejati, S., Elimelech, M., 2015. Antimicrobial properties of graphene oxide nanosheets: why size matters. Acs Nano 9 (7), 7226–7236.
Petridis, C., Konios, D., Stylianakis, M.M., Kakavelakis, G., Sygletou, M., Savva, K., Tzourmpakis, P., Krassas, M., Vaenas, N., Stratakis, E., Kymakis, E., 2016. Solution processed reduced graphene oxide electrodes for organic photovoltaics. Nanoscale Horiz. 1, 375–382.
Poland, C.A., Duffin, R., Kinloch, I., Maynard, A., Wallace, W.A.H., Seaton, A., Stone, V., Brown, S., MacNee, W., Donaldson, K., 2008. Carbon nanotubes introduced into the abdominal cavity of mice show asbestos-like pathogenicity in a pilot study. Nat. Nanotechnol. 3 (7), 423–428.
Salavagione, H.J., Martinez, G., 2011. Importance of covalent linkages in the preparation of effective reduced graphene oxide-poly(vinyl chloride) nanocomposites. Macromol 44 (8), 2685–2692.
Savva, K., Lin, Y.H., Petridis, C., Kymakis, E., Anthopoulos, T.D., Stratakis, E., 2014. In situ photo-induced chemical doping of solution processed graphene oxide for electronic applications. J. Mater. Chem. C 2 (29), 5931–5937.
Schaak, R.E., Mallouk, T.E., 2000. Prying apart ruddlesden-popper phases: exfoliation into sheets and nanotubes for assembly of perovskite thin films. Chem. Mater. 12 (11), 3427–3434.
Schmidt, C.W., 2009. Nanotechnology-related environmental, health, and safety research examining the national strategy. Environ. Health Perspect. 117 (4), A158–A161.
Sivey, J.D., Roberts, A.L., 2012. Assessing the reactivity of free chlorine constituents Cl_2, Cl_2O, and HOCl toward aromatic ethers. Environ. Sci. Technol. 46 (46), 2141–2147.
Smith, S.C., Rodrigues, D.F., 2015. Carbon-based nanomaterials for removal of chemical and biological contaminants from water: a review of mechanisms and applications. Carbon 91, 122–143.
Stratakis, E., Savva, K., Konios, D., Petridis, C., Kymakis, E., 2014. Improving the efficiency of organic photovoltaics by tuning the work function of graphene oxide hole transporting layers. Nanoscale 6 (12), 6925–6931.
Szpyrkowicz, L., Juzzolino, C., Kaul, S.N., 2001. A comparative study on oxidation of disperse dyes by electrochemical process, ozone, hypochlorite and Fenton reagent. Water Res. 35 (9), 2129–2136.
Wang, C., Shang, C., Ni, M., Dai, J., Jiang, F., 2012a. (Photo)chlorination-induced physicochemical transformation of aqueous fullerene nC_{60}. Environ. Sci. Technol. 46 (17), 9398–9405.
Wang, L.K., Hung, Y.T., Shammas, N.K., 2006. Advanced Physicochemical Treatment Processes, Handbook of Environmental Engineering.
Wang, X.P., Liu, X.Q., Han, H.Y., 2013. Evaluation of antibacterial effects of carbon nanomaterials against copper-resistant *Ralstonia solanacearum*. Colloid. Surf. B 103, 136–142.
Wang, Y., Westerhoff, P., Hristovski, K.D., 2012b. Fate and biological effects of silver, titanium dioxide, and C_{60} (fullerene) nanomaterials during simulated wastewater treatment processes. J. Hazard. Mater. 201, 16–22.
Watts, M.J., Linden, K.G., 2007. Chlorine photolysis and subsequent OH radical production during UV treatment of chlorinated water. Water Res. 41 (13), 2871–2878.
Wu, L., Liu, L., Gao, B., Munoz-Carpena, R., Zhang, M., Chen, H., Zhou, Z., Wang, H., 2013. Aggregation kinetics of graphene oxides in aqueous solutions: experiments, mechanisms, and modeling. Langmuir 29 (49), 15174–15181.
Yang, K., Ma, Y.Q., 2010. Computer simulation of the translocation of nanoparticles with different shapes across a lipid bilayer. Nat. Nanotechnol. 5 (8), 579–583.
Zhai, H.Y., Zhang, X.R., Zhu, X.H., Liu, J.Q., Ji, M., 2014. Formation of brominated disinfection byproducts during chloramination of drinking water: new polar species and overall kinetics. Environ. Sci. Technol. 48 (5), 2579–2588.
Zhang, L., Zhou, L., Yang, M., Liu, Z., Xie, Q., Peng, H., 2013. Photo-induced free radical modification of graphene. Small 9 (8), 1134–1143.
Zurutuza, A., Marinelli, C., 2014. Challenges and opportunities in graphene commercialization. Nat. Nanotechnol. 9 (10), 730–734.
Zhao, Q., Shang, C., Zhang, X.R., Ding, G.Y., Yang, X., 2011. Formation of halogenated organic byproducts during medium-pressure UV and chlorine coexposure of model compounds, NOM and bromide. Water Res. 45 (19), 6545–6554.